

# Absorption Enhancement of Black Carbon Aerosols Constrained by Mixing-State Heterogeneity

Jinghao Zhai, Xin Yang,\* Ling Li, Bin Bai, Pengfei Liu, Yuanlong Huang, Tzung-May Fu, Lei Zhu, Zhenzhong Zeng, Shu Tao, Xiaohui Lu, Xingnan Ye, Xiaofei Wang, Lin Wang, and Jianmin Chen



Cite This: *Environ. Sci. Technol.* 2022, 56, 1586–1593



Read Online

ACCESS |

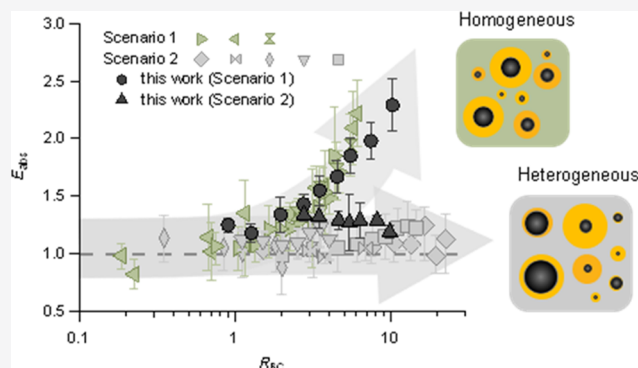
Metrics & More

Article Recommendations

Supporting Information

**ABSTRACT:** Atmospheric black carbon (BC) has a large yet highly uncertain contribution to global warming. When mixed with non-BC/coating material during atmospheric aging, the BC light absorption can be enhanced through the lensing effect. Laboratory and modeling studies have consistently found strong BC absorption enhancement, while the results in ambient measurements are conflicting, with some reporting weak absorption enhancement even for particles with large bulk coating amounts. Here, from our direct field observations, we report both large and minor absorption enhancement factors for different BC-containing particle populations with large bulk non-BC-to-BC mass ratios. By gaining insights into the measured coating material distribution across each particle population, we find that the level of absorption enhancement is strongly dependent on the particle-resolved mixing state. Our study shows that the greater mixing-state heterogeneity results in the larger difference between observed and predicted absorption enhancement. We demonstrate that by considering the variability in coating material thickness in the optical model, the previously observed model measurement discrepancy of absorption enhancement can be reconciled. The observations and improved optical models reported here highlight the importance of mixing-state heterogeneity on BC's radiative forcing, which should be better resolved in large-scale models to increase confidence when estimating the aerosol radiation effect.

**KEYWORDS:** black carbon, mixing state, absorption enhancement, radiative forcing, climate change



## 1. INTRODUCTION

Black carbon (BC) is the dominant light-absorbing component of atmospheric aerosol, while its contribution to global radiative forcing is inadequately quantified.<sup>1</sup> Along with atmospheric processes such as condensation and oxidation, freshly emitted BC with an aggregate structure is gradually coated, forming the internal mixing state of BC-containing particles.<sup>2,3</sup> Internally mixed particles with a core–shell structure can refract more light toward the BC core through coating materials, resulting in a larger light absorption cross-section than uncoated BC, referred to as the “lensing effect”.<sup>4,5</sup> The core–shell Mie theory, in which BC is treated as a spherical core and surrounded by a uniform non-BC coating,<sup>6</sup> predicts that the theoretical absorption enhancement factor ( $E_{\text{abs}}$ ) increases monotonically with an increasing non-BC-to-BC mass ratio ( $R_{\text{BC}}$ ).<sup>4</sup> Laboratory experiments of  $E_{\text{abs}}$  using monodisperse BC seeds or typical BC sources show consistency with theoretical results.<sup>7–10</sup> However, field measurements have observed both large and negligible  $E_{\text{abs}}$  for BC at high  $R_{\text{BC}}$  (Figure 1, Scenario 1 and 2).<sup>8–13</sup> The discrepancy between observational and theoretical results of  $E_{\text{abs}}$  can bring large uncertainty in quantifying BC's

contribution to the aerosol direct radiative effect. A more adequate understanding of BC light absorption enhancement should be warranted.

Several plausible mechanisms have been proposed to explain the discrepancy. From a single-particle level, the assumption of spherical morphology and a core–shell configuration might overestimate the  $E_{\text{abs}}$  of incompletely coated BC in theoretical calculation.<sup>14,15</sup> Thus, more realistic morphology treatments on ambient BC-containing particles might help solve the  $E_{\text{abs}}$  discrepancy. However, the overestimation of modeled  $E_{\text{abs}}$  caused by the incomplete and irregular coating happens only for particles at low  $R_{\text{BC}}$ .<sup>16</sup> The observed small  $E_{\text{abs}}$  of particles with high  $R_{\text{BC}}$  at high atmospheric oxidation conditions remain unexplained. In bulk measurements, particles are assumed to contain identical mass fractions which might cause an artificial

Received: September 13, 2021

Revised: December 16, 2021

Accepted: January 7, 2022

Published: January 18, 2022



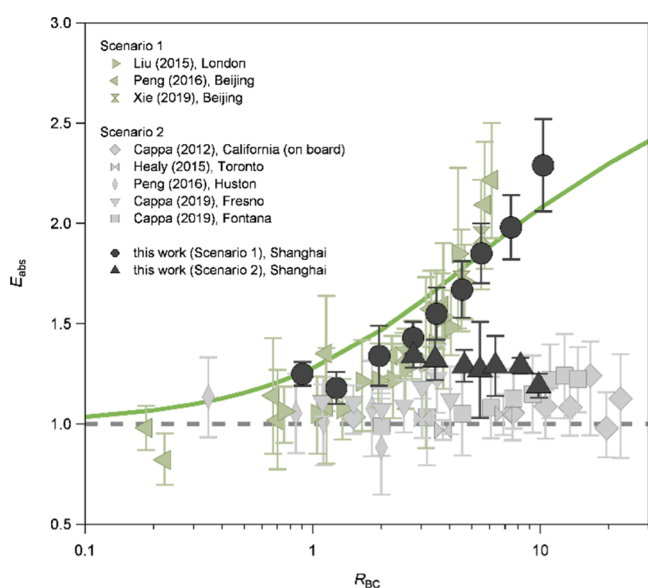


**Figure 1.** Observed absorption enhancement as a function of non-BC-to-BC mass ratio from various field measurements. For all studies, the absorption enhancements ( $E_{\text{abs}}$ ) observed at the longest wavelength are compiled. RCT was used to calculate an equivalent non-BC-to-BC mass ratio ( $R_{\text{BC}}$ ) in ref 9 and this work. Error bars denote a standard deviation of the observations for each  $R_{\text{BC}}$  interval. The green line corresponds to the core-shell Mie theory modeled result of BC-containing particles with 200 nm in size.

homogeneity across particles over the entire population and result in an overestimated  $E_{\text{abs}}$ . Recent modeling studies propose that the particle-to-particle compositional heterogeneity has an impact on population-level  $E_{\text{abs}}$ .<sup>17–19</sup>

Here, for the first time, we directly observed both large and minor BC absorption enhancement factors with high  $R_{\text{BC}}$  during different periods in a field campaign. We performed simultaneous observations of absorption enhancement, single-particle chemical composition, and mixing-state distribution of BC-containing particles at an urban site in Shanghai, China. The results suggest that, for different particle populations, the level of particle  $E_{\text{abs}}$  is strongly dependent on the heterogeneity in coating thickness. By taking into account the distribution of BC coating thickness derived from direct field measurements, the core-shell Mie model can successfully predict  $E_{\text{abs}}$  consistent with the observations. Our study highlights the importance of heterogeneity in mixing-state distribution across a BC-containing particle population to the prediction of the absorption enhancement factor. These results help to constrain one of the largest remaining uncertainties in global radiative forcing assessment.

## 2. METHODS

**2.1. Overview of the Field Campaign and Instrumentation.** The field observations were conducted at Fudan University (31°14' N, 121°29' E) in urban Shanghai, China, from 1 January to 19 January 2017. The sampling site is located in the downtown of Shanghai, close to both residential and traffic emissions. The schematic of the instrumentation is provided in Figure S1. Aerosols were dried by diffusion drying tubes before reaching the following instrumentation. Overall, the instrumentation includes measurements of optical properties, chemical compositions, and mixing states of the ambient particles. The measurement of single-particle chemical

composition started on 7 January because of the instrument maintenance.

The separation of volatile and less volatile particle components at specific temperatures was achieved by laboratory-made thermodenuders (TDs) set at 300 °C. In this work, two sets of TDs were utilized. One (TD1) was in series with the chemical and optical measurements, the other one (TD2) was used in the particle mixing-state measurements. Particle loss was calibrated to reduce the uncertainty brought by the thermophoretic forces and diffusion during the heating process.<sup>20,21</sup> Detailed description and parameters used for the TDs are given in Supporting Information and Figure S2.

Chemical composition at the single-particle level was obtained by a single-particle aerosol mass spectrometer (SPAMS, Hexin Analytical Instrument). Detailed information on the SPAMS has been described elsewhere.<sup>22,23</sup> Elemental carbon (EC) ions have been considered as important markers for BC aerosols.<sup>24</sup> Thus, BC-containing particles were selected by identifying signals of EC clusters ( $C_n^{+/-}$ ). According to the similarities of mass spectra, the BC-containing particles were classified using an adaptive resonance theory-based clustering method (ART-2a).<sup>25</sup> Based on the mass spectral patterns and chemical similarities, the BC-containing particle clusters resulting from ART-2a were then grouped into four types: BC-EC, BC-nitrate, BC-sulfate, and BC-organic carbon (OC). The averaged mass spectra of the 4 BC-containing types are shown in Figure S3.

An inhouse-built cavity ring-down spectrometer (CRDS) at 532 nm wavelength was in series with an integrating nephelometer (model 3563, TSI Inc.) to monitor extinction coefficient ( $b_{\text{ext}}$ ) and scattering coefficient ( $b_{\text{scat}}$ ) of ambient aerosols. The absorption coefficient ( $b_{\text{abs}}$ ) is then obtained by  $b_{\text{ext}}$  subtracting  $b_{\text{scat}}$ . Detailed information about our CRDS has been reported previously.<sup>26,27</sup> The aerosol scattering coefficient is measured by an integrating nephelometer at three different wavelengths (450, 550, and 700 nm) with a flowrate of 1.5 L  $\text{min}^{-1}$ . Zero adjusting is done automatically every 1 h. The nephelometer is calibrated with filtered air and  $\text{CO}_2$  gas.<sup>28</sup>

Every 10 min, the CRDS-Nephelometer system switched between the bypass and TD1 heated line. The observed light absorption enhancement factor ( $E_{\text{abs,observed}}$ ) is calculated as the ratio of the particle absorption coefficient in bypass line ( $b_{\text{abs,bypass}}$ ) to the TD line ( $b_{\text{abs,TD}}$ )

$$E_{\text{abs,observed}} = \frac{(b_{\text{abs,bypass}}(t-1) + b_{\text{abs,bypass}}(t+1))/2}{b_{\text{abs,TD}}(t)} \quad (1)$$

A self-designed volatility tandem differential mobility analyzer (V-TDMA) is employed to detect the mixing-state distribution of particles. Detailed information on the V-TDMA system has been provided elsewhere.<sup>29,30</sup> There are non-BC particles that are low-volatile and still exist after heating.<sup>31</sup> To reduce the uncertainty brought by the entire evaporation of non-BC particles after heating, we further checked the fractions of BC-containing particles from the SPAMS (see Supporting Information and Figure S4).

**2.2. Mixing State and Particle-Resolved Core-Shell Mie Model.** Assuming that a BC-containing particle is in a “core-shell” configuration and the volatile coating volume is equally distributed around a BC core, the mass ratio of volatile

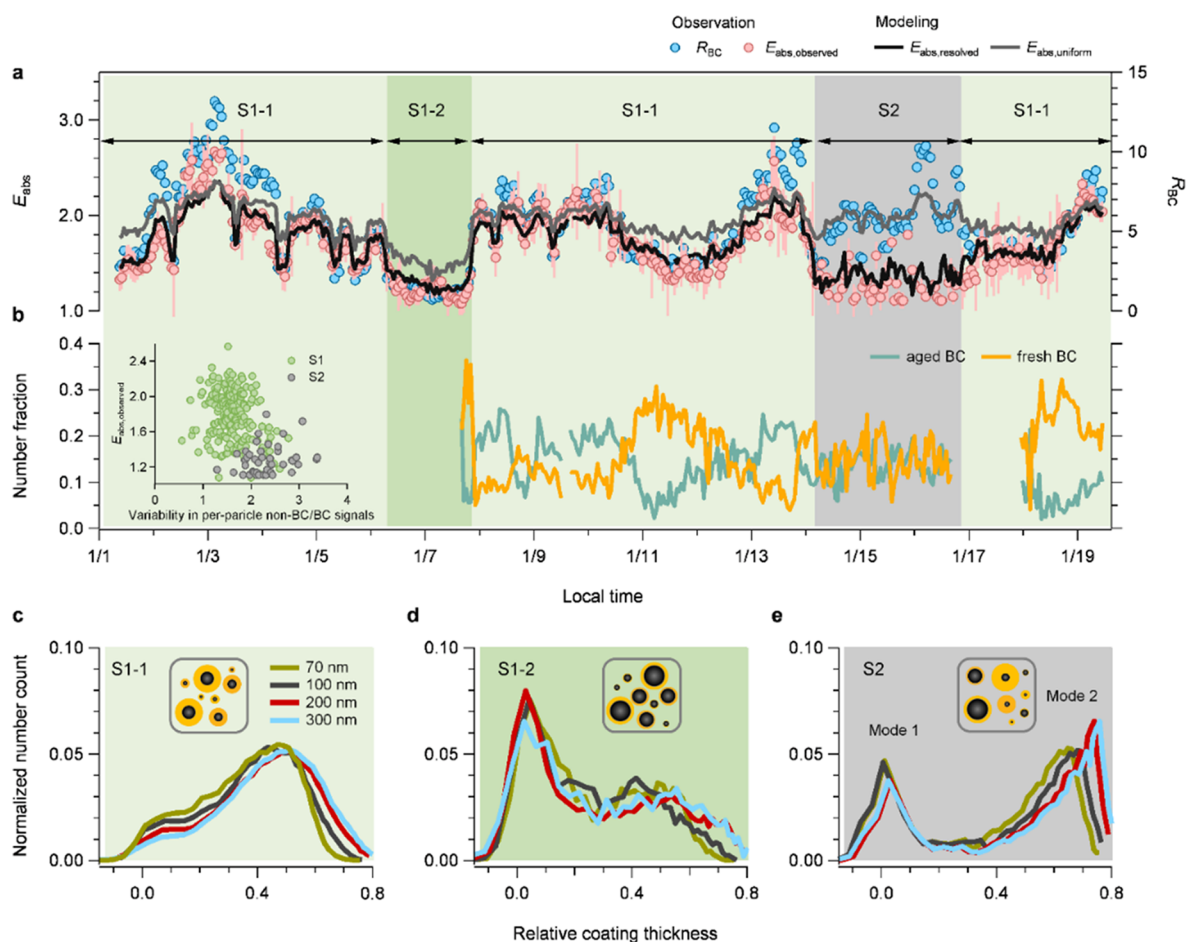


**Figure 2.** Mixing-state-dependent absorption enhancement of BC-containing particles. (a) Time series of observed absorption enhancement ( $E_{\text{abs,observed}}$ ) and core-shell Mie theory modeled absorption enhancement based on uniform coating thickness ( $E_{\text{abs,uniform}}$ ) and RCT distribution ( $E_{\text{abs,resolved}}$ ), respectively (left axis). Time series of  $R_{\text{BC}}$  is shown as well (right axis). Error bars denote a standard deviation. (b) Time series of number fractions for different BC-containing particle types (aged BC and fresh BC) detected from the SPAMS. A regular sampling period is denoted as Scenario 1-1 (S1-1), and a typical clean episode is discriminatively marked as Scenario 1-2 (S1-2). A special episode which has small  $E_{\text{abs,observed}}$  with high  $R_{\text{BC}}$  is denoted as Scenario 2 (S2). The inset in b shows the variability in non-BC/BC signal ratios of single particles from the SPAMS as a function of  $E_{\text{abs,observed}}$  for Scenario 1 and Scenario 2. (c–e) Average RCT distribution detected by the V-TDMA system for S1-1 (c), S1-2 (d), and S2 (e), respectively. Particles selected by different mobility diameters are shown with different colors. Insets in (c–e) are the illustrations of coating material distribution of BC-containing particles, as insets in (c,d) for homogeneous coating material distribution and inset e for heterogeneous coating material distribution.

coating material and non-volatile BC core ( $R_{\text{BC}}$ ) can be calculated as

$$R_{\text{BC}} = \frac{M_{\text{coating}}}{M_{\text{core}}} = \frac{(V_{\text{particle}} - V_{\text{core}})\rho_{\text{coating}}}{V_{\text{core}}\rho_{\text{core}}} = \frac{(d_{\text{particle}}^3 - d_{\text{core}}^3)\rho_{\text{coating}}}{d_{\text{core}}^3\rho_{\text{core}}} \quad (2)$$

where  $M_x$ ,  $V_x$ , and  $\rho_x$  are mass, volume, and material density, respectively.  $\rho_{\text{core}}$  and  $\rho_{\text{coating}}$  are assumed to be 1.8 and 1.5 g cm<sup>-3</sup>, respectively.<sup>8</sup> Note that the assumption here is based on the sphere core-shell configuration, thus the volume equivalent diameter  $d_x$  in the equation given above equals the particle mobility diameter. Detailed calculation and schematics of the  $R_{\text{BC}}$  based on the V-TDMA data are provided in Supporting Information and Figures S5 and S6.

The core-shell Mie model is used to calculate the theoretical  $E_{\text{abs}}$  for BC-containing particles. The Mie calculations were performed using the Matlab code developed

by Mätzler (2002)<sup>32</sup> and based on the Fortran code of Bohren and Huffman (1998).<sup>33</sup> Input parameters required in the model include the sizes and number concentrations of the BC-containing particle and the inner BC core and the refractive indexes of the BC core and coating materials. Here, the refractive indexes for BC core and coating are assumed to be  $1.88 + 0.8i$  and  $1.5 + 0.01i$  at 532 nm, respectively.<sup>8,11</sup> The sizes of the BC-containing particle and the inner BC core were applied from the diameters detected by the V-TDMA system.

For the DMA1 selected particles ( $d_p$ : 40, 70, 100, 150, 200, 300, and 350 nm), the inner core size can be derived either by considering the bulk  $R_{\text{BC}}$  or by applying the residual particles size distribution ( $d_c$ ) from the DMA2-CPC system. Detailed calculations for both cases are given in Supporting Information. The schematic of various diameters detected from the V-TDMA system and their corresponding function used in the  $R_{\text{BC}}$  and  $E_{\text{abs}}$  calculation are shown in Figure S7.

**2.3. Simulations of Relative Coating Thickness Distribution.** The shrink factor (SF) represents the BC core size ( $d_c$ ) relative to the total BC-containing particle size

( $d_p$ ). Thus, the distribution of SF can reflect the relative coating thickness (RCT) distribution ( $1 - d_c/d_p$ ) reversely. In this work, the simulated RCT distribution is assumed to be a combination of two Gaussian distributions. The bimodal Gaussian distribution follows the function of

$$f(x) = \frac{A_1}{\sqrt{2\pi}\sigma_1} \exp\left(-\frac{(x - \mu_1)^2}{2\sigma_1^2}\right) + \frac{A_2}{\sqrt{2\pi}\sigma_2} \exp\left(-\frac{(x - \mu_2)^2}{2\sigma_2^2}\right) \quad (3)$$

here,  $\mu_i$  is the mathematical expectation value of total variables which determines the mode center,  $\sigma_i$  is the standard deviation that relates to the mode dispersion, and  $A_i$  is the magnification which decides the mode area. Simulations by adjusting these parameters were made to produce the RCT distributions (Figure S8).

The simulated RCT distribution was then put into the core-shell Mie theory model to calculate the corresponding  $E_{\text{abs,resolved}}$  and  $E_{\text{abs,uniform}}$ . The single-variable controlled results of  $E_{\text{abs,resolved}}$ ,  $E_{\text{abs,uniform}}$ , and their differences (denoted by  $\Delta E_{\text{abs}}$ ) are shown in Figure S9. The  $E_{\text{abs,uniform}}$  are generally larger than the corresponding  $E_{\text{abs,resolved}}$ . As  $\sigma_2$  increases from 0.01 to 0.3,  $\Delta E_{\text{abs}}$  shows little change. However,  $\Delta E_{\text{abs}}$  becomes prominent as  $\mu_2$  increases, which leads to two further apart modes, and when  $A_2/A_1$  is  $\sim 1$ , which represents two comparable modes. That is, when the areas of the two modes are comparable, the RCT is more diverse, leading to larger discrepancy between the particle-resolved and uniformly coated particle absorption enhancement results. In this work, the variability in RCT was calculated based on the variance of the bimodal normal mixture (see Supporting Information and Figure S10).

### 3. RESULTS AND DISCUSSION

**3.1. Direct Observations of Large and Minor  $E_{\text{abs}}$ .** In this work, the observed absorption enhancement factor ( $E_{\text{abs,observed}}$ ) is calculated as the ratio between absorption coefficient of ambient particles and that of particles heated at 300 °C in a TD. The absorption coefficient of heated particles was corrected by the TD transport efficiency and residual BC-containing fractions to reduce the uncertainties due to particle loss and the entirely evaporated non-BC particles (see Supporting Information).<sup>34</sup>

On average,  $E_{\text{abs,observed}}$  during the sampling period in winter Shanghai is  $1.69 \pm 0.35$ . For most of the time (Scenario 1-1, light green shading in Figure 2),  $E_{\text{abs,observed}}$  and  $R_{\text{BC}}$  show synchronized changes, including a relative clean period with small  $E_{\text{abs,observed}}$  and low  $R_{\text{BC}}$  (Scenario 1-2, dark green shading in Figure 2). However, a special episode (Scenario 2, gray shading in Figure 2) between 1/14/2017 and 1/16/2017 leaps out with decoupling between  $E_{\text{abs,observed}}$  and  $R_{\text{BC}}$  (average data shown in Table S1).

Some previous studies have observed large  $E_{\text{abs}}$  in both rural and urban areas with moderate  $R_{\text{BC}}$ , which are consistent with the  $R_{\text{BC}}$  constrained core-shell Mie calculations.<sup>9,11,13</sup> In contrast, negligible  $E_{\text{abs}}$  are reported in some other observations, even for high  $R_{\text{BC}}$ <sup>8-10,12</sup> (Figure 1). In this work, we directly observed both large and minor  $E_{\text{abs}}$  for  $R_{\text{BC}}$  up to  $\sim 10$  during sampling periods influenced by different air masses. Overall, the relationship of  $E_{\text{abs,observed}}$  and  $R_{\text{BC}}$  in Scenario 1 shows consistent results with that from the core-

shell Mie theory calculations, whereas the results in Scenario 2 show discrepancy with Scenario 1 and fall behind the model prediction (Figure 1). Previous studies proposed that the misapplication of the complete core-shell structure approximation could be the reason for model measurement discrepancy.<sup>16,35-37</sup> While the partially coated states of BC can exist during the early stage of particle aging, such a mechanism alone is insufficient to explain the small  $E_{\text{abs}}$  observed for particles with large coating amounts ( $R_{\text{BC}}$  of  $\sim 10$ ).

**3.2. Role of Mixing-State Heterogeneity in  $E_{\text{abs}}$ .**  $E_{\text{abs}}$  for a population of BC-containing particles can be affected by its accumulated coating in bulk as well as the particle-to-particle variation in coating thickness, that is, the heterogeneity in the BC mixing state. A possible explanation of the small  $E_{\text{abs}}$  observed at high  $R_{\text{BC}}$  was explored based on coating thickness distribution of BC-containing particles derived from the measurements by V-TDMA. The polydisperse particle population was size-selected, and the distribution of SF was measured as the ratio of uncoated particle size ( $d_c$ ) distribution after heating at 300 °C to the selected size ( $d_p$ ) of unheated particles. The distribution of particle SF was then transformed to the distribution of RCT ( $\text{RCT} = (d_p - d_c)/d_p = 1 - \text{SF}$ ; see Methods).

In Scenarios 1-1 and 1-2, the RCT distributions of BC-containing particles are approximately unimodal with peak values of  $\sim 0.5$  and  $\sim 0.05$ , respectively (Figure 2, panels c,d). However, in Scenario 2, a bimodal distribution is obtained with RCT peaking at  $\sim 0.04$  for Mode 1 and  $\sim 0.63-0.75$  for Mode 2. The bimodal RCT distribution implies unevenly distributed coating material across the particle population and a large particle-to-particle variation in coating thickness. The HYSPLIT (Hybrid Single-Particle Lagrangian Integrated Trajectory model) back-trajectory model analysis shows the air mass in Scenario 2 originated from the north part of China (Figure S11). The long-range transported air mass reached the near-ground level ( $< 100$  m)  $\sim 6$  h before arriving at the sampling site. We attribute the two RCT modes in Scenario 2 to two distinct sources: (1) the local traffic emissions from urban Shanghai and (2) the long-range transported particles from northern China. The local BC-containing particles in urban Shanghai are dominated by the barely or thinly coated BC particles from fresh local traffic emissions (i.e., Mode 1), whereas the long-range transport air masses from northern China passed across the densely coal-burning and industrial areas, taking along BC-containing particles that are deeply aged with thick coatings (i.e., Mode 2).

The heterogeneity of BC coating was also confirmed by the particle-resolved mixing-state measurements from the SPAMS (see Methods). In this work, the BC-containing particles were classified into four types (BC-nitrate, BC-EC, BC-sulfate, and BC-OC) based on the similarities of single-particle mass spectra patterns obtained from the SPAMS (Figure S3). Among these four types, BC-nitrate with abundant inorganic ammonium nitrate and BC-EC with clear EC clusters were selected to represent the aged BC with thick coating and the freshly emitted BC with thin coating, respectively. The fractions of aged BC and fresh BC are well inversely correlated with each other, whereas the values are comparable in Scenario 2 (Figure 2b). The lack of a dominant mode of the mixing state for BC-containing particles in Scenario 2 causes a larger variability in particle RCT compared with Scenario 1. We further treated each time slice of the measurements during our

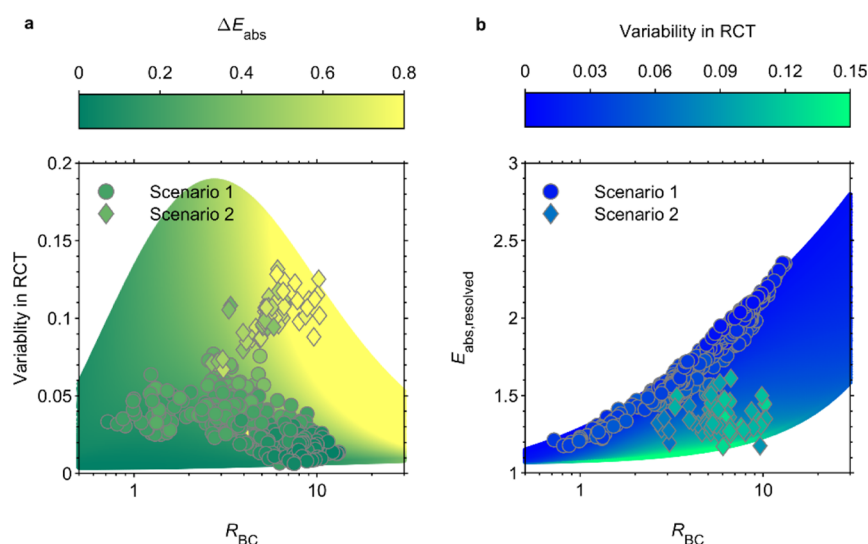


**Figure 3.** Variability in particle RCT and its constraints on the absorption enhancement. (a) Variability in particle RCT as a function of  $R_{BC}$ . All the data are colored by the absorption enhancement difference ( $\Delta E_{abs}$ ) between  $E_{abs,uniform}$  and  $E_{abs,resolved}$ . (b)  $E_{abs,resolved}$  as a function of  $R_{BC}$ . All the data are colored by the variability in RCT both for simulations and observations. Surface and scatters are the simulated and experimental data (circles for Scenario 1 and diamonds for Scenario 2), respectively.

field campaign as a particle population and analyzed the non-BC to BC signal ratios from individual particle mass spectra in each population. The variability of per-particle non-BC/BC signal ratios within a population is determined by the coefficient of variation (see Supporting Information). The variability in per-particle non-BC/BC signal ratios of Scenario 2 is generally larger than that of Scenario 1, indicating more diverse particle mixing states in Scenario 2 (inset in Figure 2b).  $E_{abs,observed}$  tends to be small for a larger variability in per-particle non-BC/BC signal ratios, which shows the underlying constraints of mixing-state heterogeneity on the particle absorption enhancement.

We calculated  $E_{abs}$  using the core-shell Mie theory based on both the classical uniformly distributed coating hypothesis and the particle-resolved coating distribution from observations. The scenario of enhanced absorption by the uniformly distributed coating was modeled based on the  $R_{BC}$  to generate the absorption enhancement ( $E_{abs,uniform}$ ). Under the assumption of equally distributed coating material across the particle population, it is expected that the ensemble-average  $E_{abs}$  from mixing effects (i.e., lensing) should increase with  $R_{BC}$ . However, the observed dependence of  $E_{abs,observed}$  on  $R_{BC}$  does not consistently follow the modeling data in Scenario 2. The RCT-corrected distribution of particle diameter was then put into the core-shell Mie theory to calculate the particle-resolved absorption enhancement ( $E_{abs,resolved}$ ). Compared to  $E_{abs,uniform}$ , the  $E_{abs,resolved}$  values agree better with the observations (see Figure 2a), suggesting the observed small  $E_{abs}$  here and possibly in other studies<sup>8–10,12</sup> at relatively high  $R_{BC}$  is likely the result of heterogeneous coating material distribution within the BC particle population.

### 3.3. Sensitivity of $E_{abs}$ on the Variability in RCT.

Further simulations were made to quantify the sensitivity of  $E_{abs}$  on the variability in RCT. We assumed that the RCT distribution was a combination of two Gaussian distributions, similar to that observed in Figure 2e (i.e., Modes 1 and 2). The function of a Gaussian mode  $i$  ( $i = 1, 2$ ) was defined by its magnification ( $A_i$ ), mathematical expectation value ( $\mu_i$ ), and standard deviation ( $\sigma_i$ ), which determine the mode area,

center, and dispersion, respectively. We made simulations by adjusting these six parameters to produce a wide range of RCT distributions (Figure S3). To further reduce the parameter space, the variability of a bimodal RCT distribution was calculated based on the Gaussian parameters (see Methods) and this reduced single parameter can reflect the diversity of mixing state across the particle population. The limit values for parameters in the simulations were based on our field observations. The simulated RCT distribution were then applied into the core-shell Mie model to calculate the corresponding  $E_{abs,resolved}$  and  $E_{abs,uniform}$ . We further calculated the difference between  $E_{abs,uniform}$  and  $E_{abs,resolved}$ , denoted by  $\Delta E_{abs}$ , to represent the uncertainty induced by the lack of information on the mixing-state distribution.

At a given  $R_{BC}$ , the  $\Delta E_{abs}$  increases with larger variability in RCT (Figure 3a). The largest variabilities of the simulated RCT distributions correspond to  $\mu_2 > 0.6$  and  $A_2/A_1 \sim 1$  (Figure S10), and  $\Delta E_{abs}$  here is remarkable as the gap between two comparable RCT modes plays an important role. In our field observation, the particle populations from long-range transport with thick coating and fresh local emission in Scenario 2 is a representative of such a condition (diamonds in Figure 3). The large variability in RCT with high  $R_{BC}$  can result in a large error in the calculated  $E_{abs}$  using the classical model with a uniform coating assumption. By considering the variability in RCT, the model measurement discrepancy is largely reconciled (Figure 3b).

The sensitivity test of  $E_{abs}$  on the variability in RCT here provides a quantitative understanding of the impact of coatings on absorption by BC-containing particles. To better evaluate the BC's radiative effects, we suggest that the particle-resolved mixing state or particle-resolved coating thickness should be added or modified as an important variable in the large-scale global climate and radiative transfer models. Basically, the distribution of particle mixing-state/RCT could be an assumption of a bimodal with one mode fixed (the fresh mode) and the other one adjustable (the aged mode).

**3.4. Atmospheric Implication.** The direct field observation of both large (up to  $\sim 2.67$ ) and minor (as small as  $\sim 1.07$ )

$E_{\text{abs}}$  values for particles with large bulk coating amounts here showed the level of  $E_{\text{abs}}$  within a particle population is strongly dependent on the variability in the particle-resolved mixing state. We demonstrate that the optical model considering the heterogeneity in coating material thickness within particle populations can reconcile the previously observed model measurement discrepancy of absorption enhancement.

Though previous studies have reported the irregular and incomplete coated morphology of BC-containing particles can lead to misestimation of  $E_{\text{abs}}$  by the core-shell-structure models,<sup>16,35–37</sup> this rationale alone cannot explain the large  $E_{\text{abs}}$  observed for particles with large bulk coating amounts. Particle-resolved mixing-state measurements and the derived optical properties help understand the impacts of BC coatings on the absorption.<sup>38</sup> Recent studies argue from a model perspective that the radiative absorption of BC is highly sensitive to the size distribution of emitted BC and particle-scale diversity in composition.<sup>17–19</sup> Our direct observations and improved optical model simulations presented herein take a step further to highlight the importance of heterogeneity in BC coating on  $E_{\text{abs}}$ , in addition to  $R_{\text{BC}}$ . However, for most large-scale global climate and aerosol models, such information has been omitted or oversimplified. We suggest that, in addition to reducing the uncertainties of BC radiative effects raised from the emission mass loading, aerosol-cloud interactions, and so forth,<sup>39</sup> the particle mixing-state heterogeneity (more specifically, the particle RCT distribution, or the core and total size distribution) should be better resolved in field studies as well as in global modeling of aerosol radiative forcing.

## ■ ASSOCIATED CONTENT

### SI Supporting Information

The Supporting Information is available free of charge at <https://pubs.acs.org/doi/10.1021/acs.est.1c06180>.

Detailed description of thermo-desorption, single-particle chemical composition, optical measurements, mixing state, the  $R_{\text{BC}}$  calculation, particle-resolved core-shell Mie model, and variability in RCT distribution (PDF)

## ■ AUTHOR INFORMATION

### Corresponding Author

**Xin Yang** – School of Environmental Science and Engineering, Southern University of Science and Technology, Shenzhen 518055, China; [orcid.org/0000-0002-9173-1188](https://orcid.org/0000-0002-9173-1188);  
Email: [yangx@sustech.edu.cn](mailto:yangx@sustech.edu.cn)

### Authors

**Jinghao Zhai** – School of Environmental Science and Engineering, Southern University of Science and Technology, Shenzhen 518055, China; [orcid.org/0000-0001-9538-2299](https://orcid.org/0000-0001-9538-2299)

**Ling Li** – Shanghai Key Laboratory of Atmospheric Particle Pollution and Prevention, Department of Environmental Science and Engineering, Fudan University, Shanghai 200433, China

**Bin Bai** – School of Earth and Atmospheric Sciences, Georgia Institute of Technology, Atlanta, Georgia 30332, United States

**Pengfei Liu** – School of Earth and Atmospheric Sciences, Georgia Institute of Technology, Atlanta, Georgia 30332, United States

**Yuanlong Huang** – Division of Geological and Planetary Sciences, California Institute of Technology, Pasadena, California 91125, United States; [orcid.org/0000-0002-6726-8904](https://orcid.org/0000-0002-6726-8904)

**Tzung-May Fu** – School of Environmental Science and Engineering, Southern University of Science and Technology, Shenzhen 518055, China; [orcid.org/0000-0002-8556-7326](https://orcid.org/0000-0002-8556-7326)

**Lei Zhu** – School of Environmental Science and Engineering, Southern University of Science and Technology, Shenzhen 518055, China

**Zhenzhong Zeng** – School of Environmental Science and Engineering, Southern University of Science and Technology, Shenzhen 518055, China

**Shu Tao** – School of Environmental Science and Engineering, Southern University of Science and Technology, Shenzhen 518055, China; Laboratory for Earth Surface Process, College of Urban and Environmental Sciences, Peking University, Beijing 100871, China; [orcid.org/0000-0002-7374-7063](https://orcid.org/0000-0002-7374-7063)

**Xiaohui Lu** – Shanghai Key Laboratory of Atmospheric Particle Pollution and Prevention, Department of Environmental Science and Engineering, Fudan University, Shanghai 200433, China

**Xingnan Ye** – Shanghai Key Laboratory of Atmospheric Particle Pollution and Prevention, Department of Environmental Science and Engineering, Fudan University, Shanghai 200433, China

**Xiaofei Wang** – Shanghai Key Laboratory of Atmospheric Particle Pollution and Prevention, Department of Environmental Science and Engineering, Fudan University, Shanghai 200433, China

**Lin Wang** – Shanghai Key Laboratory of Atmospheric Particle Pollution and Prevention, Department of Environmental Science and Engineering, Fudan University, Shanghai 200433, China; [orcid.org/0000-0002-4905-3432](https://orcid.org/0000-0002-4905-3432)

**Jianmin Chen** – Shanghai Key Laboratory of Atmospheric Particle Pollution and Prevention, Department of Environmental Science and Engineering, Fudan University, Shanghai 200433, China; [orcid.org/0000-0001-5859-3070](https://orcid.org/0000-0001-5859-3070)

Complete contact information is available at:

<https://pubs.acs.org/10.1021/acs.est.1c06180>

### Notes

The authors declare no competing financial interest.

## ■ ACKNOWLEDGMENTS

This work was supported by the National Natural Science Foundation of China (41827804, 41775150, and 91544224) and Guangdong Provincial Research and Development Plan in Key Area (2020B1111360001) and Shanghai Environmental Monitoring Centre.

## ■ REFERENCES

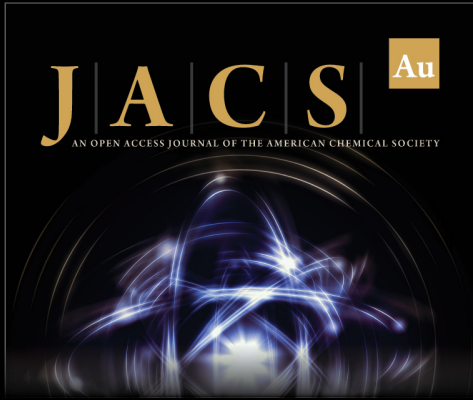
- (1) Ramanathan, V.; Carmichael, G. Global and regional climate changes due to black carbon. *Nat. Geosci.* **2008**, *1*, 221–227.
- (2) Shiraiwa, M.; Kondo, Y.; Moteki, N.; Takegawa, N.; Miyazaki, Y.; Blake, D. R. Evolution of mixing state of black carbon in polluted air from Tokyo. *Geophys. Res. Lett.* **2007**, *34*, L16803.

- (3) China, S.; Mazzoleni, C.; Gorkowski, K.; Aiken, A. C.; Dubey, M. K. Morphology and mixing state of individual freshly emitted wildfire carbonaceous particles. *Nat. Commun.* **2013**, *4*, 2122.
- (4) Bond, T. C.; Habib, G.; Bergstrom, R. W. Limitations in the enhancement of visible light absorption due to mixing state. *J. Geophys. Res.: Atmos.* **2006**, *111*, D20211.
- (5) Fuller, K. A.; Malm, W. C.; Kreidenweis, S. M. Effects of mixing on extinction by carbonaceous particles. *J. Geophys. Res.: Atmos.* **1999**, *104*, 15941–15954.
- (6) Jacobson, M. Z. Strong radiative heating due to the mixing state of black carbon in atmospheric aerosols. *Nature* **2001**, *409*, 695–697.
- (7) Schnaiter, M.; Linke, C.; Mohler, O.; Naumann, K. H.; Saathoff, H.; Wagner, R.; Schurath, U.; Wehner, B. Absorption amplification of black carbon internally mixed with secondary organic aerosol. *J. Geophys. Res.: Atmos.* **2005**, *110*, D19204.
- (8) Cappa, C. D.; Onasch, T. B.; Massoli, P.; Worsnop, D. R.; Bates, T. S.; Cross, E. S.; Davidovits, P.; Hakala, J.; Hayden, K. L.; Jobson, B. T.; Kolesar, K. R.; Lack, D. A.; Lerner, B. M.; Li, S.-M.; Mellon, D.; Nuaaman, I.; Olfert, J. S.; Petäjä, T.; Quinn, P. K.; Song, C.; Subramanian, R.; Williams, E. J.; Zaveri, R. A. Radiative Absorption Enhancements Due to the Mixing State of Atmospheric Black Carbon. *Science* **2012**, *337*, 1078–1081.
- (9) Peng, J.; Hu, M.; Guo, S.; Du, Z.; Zheng, J.; Shang, D.; Levy Zamora, M.; Zeng, L.; Shao, M.; Wu, Y.-S.; Zheng, J.; Wang, Y.; Glen, C. R.; Collins, D. R.; Molina, M. J.; Zhang, R. Markedly enhanced absorption and direct radiative forcing of black carbon under polluted urban environments. *Proc. Natl. Acad. Sci. U.S.A.* **2016**, *113*, 4266–4271.
- (10) Healy, R. M.; Wang, J. M.; Jeong, C.-H.; Lee, A. K. Y.; Willis, M. D.; Jaroudi, E.; Zimmerman, N.; Hilker, N.; Murphy, M.; Eckhardt, S.; Stohl, A.; Abbatt, J. P. D.; Wenger, J. C.; Evans, G. J. Light-absorbing properties of ambient black carbon and brown carbon from fossil fuel and biomass burning sources. *J. Geophys. Res.: Atmos.* **2015**, *120*, 6619–6633.
- (11) Liu, S.; Aiken, A. C.; Gorkowski, K.; Dubey, M. K.; Cappa, C. D.; Williams, L. R.; Herndon, S. C.; Massoli, P.; Fortner, E. C.; Chhabra, P. S.; Brooks, W. A.; Onasch, T. B.; Jayne, J. T.; Worsnop, D. R.; China, S.; Sharma, N.; Mazzoleni, C.; Xu, L.; Ng, N. L.; Liu, D.; Allan, J. D.; Lee, J. D.; Fleming, Z. L.; Mohr, C.; Zotter, P.; Szidat, S.; Prévôt, A. S. H. Enhanced light absorption by mixed source black and brown carbon particles in UK winter. *Nat. Commun.* **2015**, *6*, 8435.
- (12) Cappa, C. D.; Zhang, X.; Russell, L. M.; Collier, S.; Lee, A. K. Y.; Chen, C.-L.; Betha, R.; Chen, S.; Liu, J.; Price, D. J.; Sanchez, K. J.; McMeeking, G. R.; Williams, L. R.; Onasch, T. B.; Worsnop, D. R.; Abbatt, J.; Zhang, Q. Light Absorption by Ambient Black and Brown Carbon and its Dependence on Black Carbon Coating State for Two California, USA, Cities in Winter and Summer. *J. Geophys. Res.: Atmos.* **2019**, *124*, 1550–1577.
- (13) Xie, C.; Xu, W.; Wang, J.; Liu, D.; Ge, X.; Zhang, Q.; Wang, Q.; Du, W.; Zhao, J.; Zhou, W.; Li, J.; Fu, P.; Wang, Z.; Worsnop, D.; Sun, Y. Light absorption enhancement of black carbon in urban Beijing in summer. *Atmos. Environ.* **2019**, *213*, 499–504.
- (14) Moteki, N.; Kondo, Y.; Adachi, K. Identification by single-particle soot photometer of black carbon particles attached to other particles: Laboratory experiments and ground observations in Tokyo. *J. Geophys. Res.: Atmos.* **2014**, *119*, 1031–1043.
- (15) Sedlacek, A. J.; Lewis, E. R.; Kleinman, L.; Xu, J. Z.; Zhang, Q. Determination of and evidence for non-core-shell structure of particles containing black carbon using the Single-Particle Soot Photometer (SP2). *Geophys. Res. Lett.* **2012**, *39*, L06802.
- (16) Liu, D.; Whitehead, J.; Alfara, M. R.; Reyes-Villegas, E.; Spracklen, D. V.; Reddington, C. L.; Kong, S.; Williams, P. I.; Ting, Y.-C.; Haslett, S.; Taylor, J. W.; Flynn, M. J.; Morgan, W. T.; McFiggans, G.; Coe, H.; Allan, J. D. Black-carbon absorption enhancement in the atmosphere determined by particle mixing state. *Nat. Geosci.* **2017**, *10*, 184–188.
- (17) Fierce, L.; Bond, T. C.; Bauer, S. E.; Mena, F.; Riemer, N. Black carbon absorption at the global scale is affected by particle-scale diversity in composition. *Nat. Commun.* **2016**, *7*, 12361.
- (18) Fierce, L.; Onasch, T. B.; Cappa, C. D.; Mazzoleni, C.; China, S.; Bhandari, J.; Davidovits, P.; Fischer, D. A.; Helgestad, T.; Lambe, A. T.; Sedlacek, A. J.; Smith, G. D.; Wolff, L. Radiative absorption enhancements by black carbon controlled by particle-to-particle heterogeneity in composition. *Proc. Natl. Acad. Sci. U.S.A.* **2020**, *117*, 5196–5203.
- (19) Matsui, H.; Hamilton, D. S.; Mahowald, N. M. Black carbon radiative effects highly sensitive to emitted particle size when resolving mixing-state diversity. *Nat. Commun.* **2018**, *9*, 3446.
- (20) Philippin, S.; Wiedensohler, A.; Stratmann, F. Measurements of non-volatile fractions of pollution aerosols with an eight-tube volatility tandem differential mobility analyzer (VTDMA-8). *J. Aerosol Sci.* **2004**, *35*, 185–203.
- (21) Wehner, B.; Philippin, S.; Wiedensohler, A. Design and calibration of a thermodenuder with an improved heating unit to measure the size-dependent volatile fraction of aerosol particles. *J. Aerosol Sci.* **2002**, *33*, 1087–1093.
- (22) Li, L.; Huang, Z.; Dong, J.; Li, M.; Gao, W.; Nian, H.; Fu, Z.; Zhang, G.; Bi, X.; Cheng, P.; Zhou, Z. Real time bipolar time-of-flight mass spectrometer for analyzing single aerosol particles. *Int. J. Mass Spectrom.* **2011**, *303*, 118–124.
- (23) Zhai, J.; Lu, X.; Li, L.; Zhang, Q.; Zhang, C.; Chen, H.; Yang, X.; Chen, J. Size-resolved chemical composition, effective density, and optical properties of biomass burning particles. *Atmos. Chem. Phys.* **2017**, *17*, 7481–7493.
- (24) Spencer, M. T.; Prather, K. A. Using ATOFMS to Determine OC/EC Mass Fractions in Particles. *Aerosol Sci. Technol.* **2006**, *40*, 585–594.
- (25) Song, X.-H.; Hopke, P. K.; Fergenson, D. P.; Prather, K. A. Classification of single particles analyzed by ATOFMS using an artificial neural network, ART-2A. *Anal. Chem.* **1999**, *71*, 860–865.
- (26) Li, L.; Chen, J.; Chen, H.; Yang, X.; Tang, Y.; Zhang, R. Monitoring optical properties of aerosols with cavity ring-down spectroscopy. *J. Aerosol Sci.* **2011**, *42*, 277–284.
- (27) Huang, Y.; Li, L.; Li, J.; Wang, X.; Chen, H.; Chen, J.; Yang, X.; Gross, D. S.; Wang, H.; Qiao, L.; Chen, C. A case study of the highly time-resolved evolution of aerosol chemical and optical properties in urban Shanghai, China. *Atmos. Chem. Phys.* **2013**, *13*, 3931–3944.
- (28) Anderson, T. L.; Ogren, J. A. Determining Aerosol Radiative Properties Using the TSI 3563 Integrating Nephelometer. *Aerosol Sci. Technol.* **1998**, *29*, 57–69.
- (29) Ye, X.; Chen, T.; Hu, D.; Yang, X.; Chen, J.; Zhang, R.; Khakuziv, A. F.; Wang, L. A multifunctional HTDMA system with a robust temperature control. *Adv. Atmos. Sci.* **2009**, *26*, 1235–1240.
- (30) Wang, X.; Ye, X.; Chen, J.; Wang, X.; Yang, X.; Fu, T.-M.; Zhu, L.; Liu, C. Direct links between hygroscopicity and mixing state of ambient aerosols: estimating particle hygroscopicity from their single-particle mass spectra. *Atmos. Chem. Phys.* **2020**, *20*, 6273–6290.
- (31) Cheung, H. H. Y.; Tan, H.; Xu, H.; Li, F.; Wu, C.; Yu, J. Z.; Chan, C. K. Measurements of non-volatile aerosols with a VTDMA and their correlations with carbonaceous aerosols in Guangzhou, China. *Atmos. Chem. Phys.* **2016**, *16*, 8431–8446.
- (32) Mätzler, C. *MATLAB Function for Mie Scattering and Absorption*. Res. Rep. 2002-08, Institut für Angewandte Physik: Bern, 2002.
- (33) Bohren, C. F.; Huffman, D. R. *Absorption and Scattering of Light by Small Particles*; John Wiley: Hoboken, NJ, 1983; p 530.
- (34) Huffman, J. A.; Ziemann, P. J.; Jayne, J. T.; Worsnop, D. R.; Jimenez, J. L. Development and Characterization of a Fast-Stepping/Scanning Thermodenuder for Chemically-Resolved Aerosol Volatility Measurements. *Aerosol Sci. Technol.* **2008**, *42*, 395–407.
- (35) Adachi, K.; Chung, S. H.; Buseck, P. R. Shapes of soot aerosol particles and implications for their effects on climate. *J. Geophys. Res.: Atmos.* **2010**, *115*, D15206.
- (36) Chakrabarty, R. K.; Heinson, W. R. Scaling Laws for Light Absorption Enhancement Due to Nonrefractory Coating of Atmospheric Black Carbon Aerosol. *Phys. Rev. Lett.* **2018**, *121*, 218701.

(37) Wu, Y.; Cheng, T.; Liu, D.; Allan, J. D.; Zheng, L.; Chen, H. Light Absorption Enhancement of Black Carbon Aerosol Constrained by Particle Morphology. *Environ. Sci. Technol.* **2018**, *52*, 6912–6919.


(38) Liu, D. T.; Zhao, D. L.; Xie, Z. Z.; Yu, C. J.; Chen, Y.; Tian, P.; Ding, S.; Hu, K.; Lowe, D.; Liu, Q.; Zhou, W.; Wang, F.; Sheng, J. J.; Kong, S. F.; Hu, D. W.; Wang, Z. Z.; Huang, M. Y.; Ding, D. P. Enhanced heating rate of black carbon above the planetary boundary layer over megacities in summertime. *Environ. Res. Lett.* **2019**, *14*, 124003.


(39) Naik, V.; Szopa, S.; Adhikary, B.; Artaxo, P.; Berntsen, T.; Collins, W. D.; Fuzzi, S.; Gallardo, L.; Kiendler Scharr, A.; Klimont, Z.; Liao, H.; Unger, N.; Zanis, P. Short-Lived Climate Forcers. In: *Climate Change 2021: The Physical Science Basis*; Masson-Delmotte, V., Zhai, P., Pirani, A., Connors, S. L., Péan, C., Berger, S., Caud, N., Chen, Y., Goldfarb, L., Gomis, M. I., Huang, M., Leitzell, K., Lonnoy, E., Matthews, J. B. R., Maycock, T. K., Waterfield, T., Yelekçi, O., Yu, R., Zhou, B., Eds.; Cambridge University Press, 2021.



**JACS** Au  
AN OPEN ACCESS JOURNAL OF THE AMERICAN CHEMICAL SOCIETY

Editor-in-Chief  
**Prof. Christopher W. Jones**  
Georgia Institute of Technology, USA

**Open for Submissions** 

pubs.acs.org/jacsau  ACS Publications  
Most Trusted. Most Cited. Most Read.